Electrochemical CO_2 Reduction to Hydrocarbons on a Heterogeneous Molecular Cu Catalyst in Aqueous Solution

Zhe Weng,[†,‡,∥] Jianbing Jiang,[†,‡,∥] Yueshen Wu,[†,‡] Zishan Wu,[†,‡] Xiaoting Guo,[†,‡,§] Kelly L. Materna,[†,‡] Wen Liu,[†,‡] Victor S. Batista,[†,‡] Gary W. Brudvig,[*,†,‡] and Hailiang Wang[*,†,‡]

[†]Department of Chemistry, Yale University, New Haven, Connecticut 06520, United States
[‡]Energy Sciences Institute, Yale University, West Haven, Connecticut 06516, United States
[§]Department of Chemistry, Nankai University, Tianjin 300071, The People's Republic of China

Ⓢ *Supporting Information*

ABSTRACT: Exploration of heterogeneous molecular catalysts combining the atomic-level tunability of molecular structures and the practical handling advantages of heterogeneous catalysts represents an attractive approach to developing high-performance catalysts for important and challenging chemical reactions such as electrochemical carbon dioxide reduction which holds the promise for converting emissions back to fuels utilizing renewable energy. Thus, far, efficient and selective electroreduction of CO_2 to deeply reduced products such as hydrocarbons remains a big challenge. Here, we report a molecular copper-porphyrin complex (copper(II)-5,10,15,20-tetrakis-(2,6-dihydroxyphenyl)porphyrin) that can be used as a heterogeneous electrocatalyst with high activity and selectivity for reducing CO_2 to hydrocarbons in aqueous media. At −0.976 V vs the reversible hydrogen electrode, the catalyst is able to drive partial current densities of 13.2 and 8.4 mA cm^{-2} for methane and ethylene production from CO_2 reduction, corresponding to turnover frequencies of 4.3 and 1.8 molecules·site^{-1}·s^{-1} for methane and ethylene, respectively. This represents the highest catalytic activity to date for hydrocarbon production over a molecular CO_2 reduction electrocatalyst. The unprecedented catalytic performance is attributed to the built-in hydroxyl groups in the porphyrin structure and the reactivity of the copper(I) metal center.

Increasing concern about global warming and a potential energy crisis has prompted the search for new technologies for converting CO_2, a notorious greenhouse gas from fossil fuel burning, back to fuels or other value-added chemicals. One attractive proposal to achieve a carbon-neutral energy cycle is to power electrochemical CO_2 reduction with electricity generated from renewable energy sources.[1,2] Due to the high chemical inertness of CO_2 molecules and the associated multielectron transfer processes, electrochemical CO_2 reduction reactions face large energy barriers.[3,4] It is imperative to apply high-performance electrocatalysts to accelerate sluggish reaction kinetics and improve product distribution. Many materials have been found to be catalytically active for CO_2 electroreduction, including metals (e.g., Au, Ag, Cu, Zn, Sn, and Co),[5−8] metal oxides (e.g., SnO_2 and CuO),[9,10] metal chalcogenides (e.g., MoS_2),[11]

heteroatom-doped carbons (e.g., nitrogen-doped carbon nanotubes and carbon nanofibers),[12−14] and molecular compounds (metal organic complexes).[1] Despite the notable progress, it is still a great challenge to steer the reaction pathways toward desirable products and reduce reaction overpotentials, necessitating the development of better electrocatalysts with higher product selectivity and catalytic activity.

Metal organic complexes are a family of electrocatalyst materials with distinct advantages because their molecular structures can be accurately tailored for improving catalytic properties as well as investigating catalytic mechanisms. Thus, far, a large number of molecular catalysts that combine transition-metal elements such as Re, Ru, Fe, Co, Ni, Mn, Cu, Ag, Ir, and Pd with ligands such as polypyridine, phosphine, cyclam, porphyrin, phthalocyanine, and other macrocyclic structures have been studied for electrochemical reduction of CO_2.[15,16] While CO_2 electroreduction can be effectively catalyzed by these materials, the major reduction products have been CO, formic acid (or formate), and oxalic acid (or oxalate), corresponding to one or two electrons transferred to every CO_2 molecule.[17−19] Even though more deeply reduced products such as methanol and methane have been observed occasionally, they usually appeared as minor products compared to CO or formic acid.[20−24] It remains challenging for molecular electrocatalysts to promote multielectron-transfer reactions with high selectivity. In addition, most of the existing metal complex catalysts for CO_2 electroreduction are used in homogeneous catalysis conditions where the catalytically active molecules are dissolved in solution.[19] Organic solvents are needed, and the catalysts are difficult to separate and regenerate, which may limit large-scale applications. Therefore, it is both scientifically and practically appealing to explore new molecular electrocatalyst materials that can selectively convert CO_2 to deeply reduced products such as hydrocarbons under heterogeneous catalysis conditions in aqueous solutions.

Herein, we report a new copper-porphyrin complex, copper-(II)-5,10,15,20-tetrakis(2,6-dihydroxyphenyl)porphyrin (PorCu) and its distinctive catalytic properties as a heterogeneous molecular electrocatalyst for CO_2 reduction in neutral aqueous media. The PorCu catalyst manifests high activity and selectivity for electrochemical CO_2 reduction to hydrocarbons

(methane and ethylene). With a mass loading of 0.25 mg cm^{-2} and under an electrochemical potential of −0.976 V vs the reversible hydrogen electrode (RHE), our catalyst is able to convert CO_2 to hydrocarbons with a Faradaic efficiency of 44%, substantially suppressing the other CO_2 reduction pathways. An ultrahigh geometric current density of 21 mA/cm^2 for combined methane and ethylene production is achieved under the same conditions, giving turnover frequencies (TOFs) of 4.3 methane and 1.8 ethylene molecules·site^{-1}·s^{-1}. Our studies reveal that the built-in hydroxyl groups on the porphyrin ligand and the oxidation state of the Cu center are both critical factors contributing to the superior catalytic performance.

The synthetic route for the target molecule PorCu is shown in Figure 1. 5,10,15,20-tetrakis(2,6-dimethoxyphenyl)porphyrin
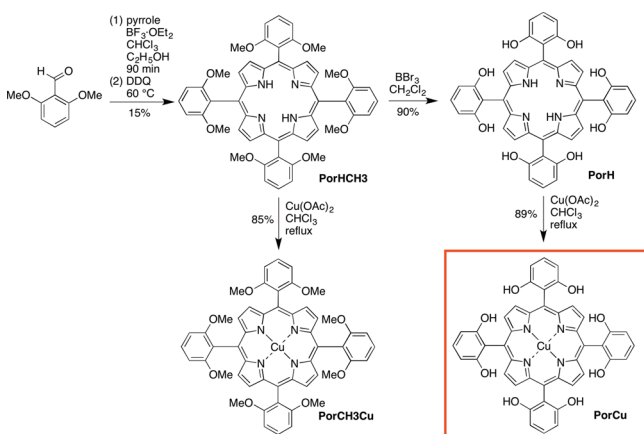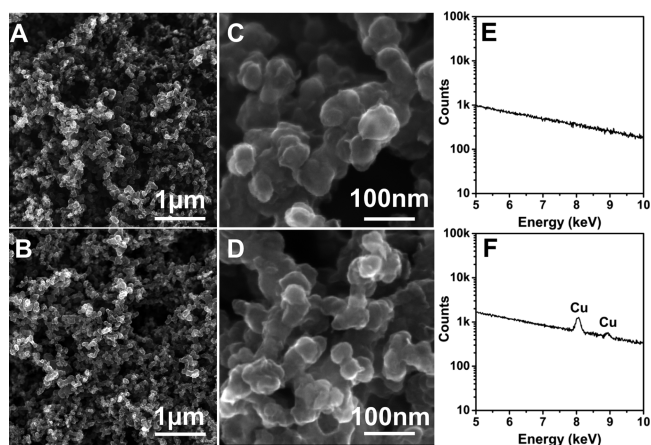
Figure 2. SEM and EDS characterizations of the PorCu catalyst electrode. SEM images of the (A,C) pristine carbon-nanoparticle-coated carbon fiber paper electrode and (B,D) PorCu deposited carbon electrode. (E,F) EDS diagrams of the pristine and PorCu deposited carbon electrodes.

Figure 1. Synthetic routes for copper−porphyrin molecular catalysts.

(PorHCH3) was first synthesized from 2,6-dimethoxybenzalde-hyde and pyrrole via the standard Lindsey procedure.[25] All the eight methyl groups were then removed by reacting the PorHCH3 with boron tribromide in dichloromethane at room temperature to afford 5,10,15,20-tetrakis(2,6-dihydroxyphenyl)-porphyrin (PorH) in 90% yield. Treatment of the PorH with copper(II) acetate in refluxing chloroform afforded the copper chelated PorCu in 89% yield. In a divergent route, the PorHCH3 was treated with copper(II) acetate in refluxing chloroform, giving copper(II) 5,10,15,20-tetrakis(2,6-dimethoxyphenyl)-porphyrin (PorCH3Cu) in 85% yield. All the porphyrin products were purified and characterized by UV−vis absorption spectros-copy, MALDI-MS, and ^{1}H and ^{13}C NMR spectroscopy (Figures S1−S3). NMR spectra were not recorded for the PorCu and PorCH3Cu due to the paramagnetic nature of copper(II).

The PorCu material was dissolved in methanol and then deposited on a commercial polytetrafluoroethylene-treated carbon fiber paper with a porous coating layer to form the catalyst electrode. The porous coating layer consisted of carbon nanoparticles with an average diameter of ∼50 nm, as shown by SEM imaging (Figure 2A,C). After PorCu deposition, no detectable morphological changes were observed for the microstructure of the substrate (Figure 2B,D), suggesting the PorCu catalyst was uniformly distributed on the carbon nanoparticles. Cu element signals were clearly detected from the PorCu loaded carbon fiber paper by EDS, unambiguously confirming the presence of the PorCu catalyst on the electrode (Figure 2E,F).

Cyclic voltammetry (CV) measurements were performed for the PorCu electrode in 0.5 M aqueous KHCO$_3$ solution

saturated with argon or CO_2. In an argon atmosphere, significant cathodic current was recorded at potentials more negative than −0.4 V vs RHE (Figure 3A dotted red trace), with hydrogen
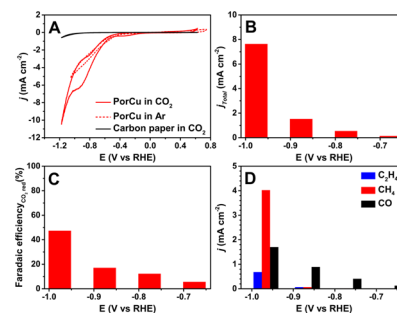
Figure 3. Electrochemical CO_2 reduction over the PorCu electrode with a catalyst mass loading of 0.25 mg cm^{-2} in aqueous 0.5 M KHCO$_3$. (A) CV curves at the scan rate of 100 mV s^{-1}. (B) Total current densities, (C) CO_2 reduction Faradaic efficiencies, and (D) distribution of CO_2 reduction products in the gas phase at various electrode potentials; all measured 8 min after electrolysis was started.

detected as the only product, thus ascribing the current to PorCu-catalyzed hydrogen evolution. A pair of weak and broad waves is visible at around −0.9 V. DFT calculations showed that the standard reduction potential of PorCu$^{0/-}$ is −0.85 V vs RHE, while that of PorCu$^{-/2-}$ is −1.14 V (computational details in SI), suggesting that the observed CV waves at around −0.9 V are likely to be associated with one-electron redox between PorCu^0 and PorCu$^-$. After the electrolyte was saturated with CO_2, a higher current density was observed (Figure 3A solid red trace), and CO_2 reduction products were detected. The same carbon fiber paper electrode without catalyst loading only exhibited negligible background current (Figure 3A black trace). Taken together, these results indicate that the PorCu has a substantial catalytic effect on electrochemical reduction of CO_2. It is worthwhile to note that the pair of redox waves became much more prominent under a CO_2 atmosphere, which indicates the possibility of CO_2 participating in the redox reaction of PorCu.

The PorCu catalyst electrodes were studied for electro-chemical CO_2 reduction in the CO_2 saturated KHCO$_3$ electrolyte under various potentials. The liquid and gas products

were analyzed by ^{1}H NMR (Figure S4) and GC-MS (Figure S5), respectively. At all the selected potentials, formic acid was the only detected liquid product, and the faradaic efficiencies were all <5% (Figure S6). Considering formic acid is always a minor product in our studies and its production rate can only be quantified in a time-averaged format after the entire electrocatalysis is completed, we will focus on the gas-phase products in our following discussions. The initial total current densities and CO_2 reduction Faradaic efficiencies are plotted in Figure 3B,C. With larger overpotentials applied to the catalyst electrodes, larger total current densities and higher CO_2 reduction Faradaic efficiencies were achieved. At −0.976 V vs RHE, the initial total current density was ∼15 mA cm^{-2}, and 47% of the electrons were directed to CO_2 reduction with the rest spent on hydrogen evolution and formic acid formation. The distribution of CO_2 reduction products was found to be dependent on the electrode potential (Figures 3D and S7). At −0.676 V vs RHE, CO was the only CO_2 reduction product. At −0.776 V a trace amount of methane was discovered in the products. At −0.876 V, CO was still the dominant CO_2 reduction product, with small fractions of methane and ethylene. Interestingly, as the catalyst electrode was further negatively polarized to −0.976 V, the yields of methane and ethylene dramatically increased, with methane being the dominant CO_2 reduction product (Figure 3D). It is noted that the production of hydrocarbons is strongly correlated with the PorCu redox waves at −0.9 V, suggesting that a reduced form of the PorCu molecules are the active catalytic sites for reducing CO_2 into methane and ethylene.

As the electrocatalysis continued at −0.976 V, the total current continuously increased until the potential at the counter electrode went beyond the measuring limit of our potentiostat in ∼1 h (Figure S8), during which the gas products were sampled at certain time points. The total current density increased from 11 to 48 mA cm^{-2} (Figure S8), and the Faradaic efficiency for CO_2 reduction to gas-phase products increased from 42% to 54% (Figure 4A). Methane and ethylene always remained as the major
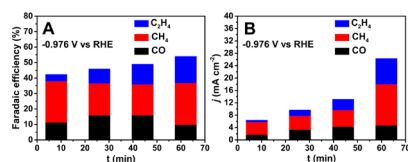

Figure 4. Distribution of CO_2 reduction products in the gas phase as the electrolysis proceeds at −0.976 V vs RHE. (A) Faradaic efficiencies and (B) partial current densities for the gas-phase products.

CO_2 reduction products. After this activation process, the catalyst electrode was able to convert CO_2 to methane and ethylene with partial current densities of 13.2 and 8.4 mA cm^{-2}, respectively (Figure 4B). The corresponding TOFs for methane and ethylene production can be calculated as 4.3 and 1.8 molecules·site^{-1}·s^{-1}, respectively. To the best of our knowledge, this is the first time for a molecular metal complex catalyst material to give such high catalytic reaction rates for hydrocarbon products at ∼−1 V vs RHE (Table S1),[20,24] which is also higher than most of the reported Cu metal based electrocatalysts at comparable overpotentials (Table S1).[26−31]

CV and EIS measurements were employed at certain time intervals to characterize the PorCu catalyst electrode, while it was being held at the potential of −0.976 V vs RHE in the CO_2 saturated KHCO$_3$ electrolyte. The CV curves were recorded in the potential window of 0.025−0.225 V vs RHE where no

Faradaic reaction took place, so that the electrochemically active surface area (ECSA) could be represented by the line slopes of the current-scan rate plots (Figure S9B−D). It is clear that the ECSA increased during the activation process, which can be an important contributor to the current density increase as more and more sites became available for catalysis. The finding was also supported by the EIS results. All the Nyquist plots exhibit straight and steep tails in the low-frequency region (Figure S9A), characteristic of capacitive behavior.[32] Increased tail slopes and decreased Nyquist tail lengths were observed during the catalyst electrode activation process, indicating facilitated electrolyte infiltration into the PorCu catalyst layer and an increased number of accessible surface sites.[32] More significant redox peaks were observed in the CV curve of the PorCu catalyst electrode after electrocatalysis (Figure S10), supporting our hypothesis that more active sites were exposed during the activation process. SEM imaging of the catalyst electrode after electrocatalysis revealed negligible changes in microstructure (Figure S11), thus excluding the possibility that morphological changes are responsible for the catalyst activation. It is worthwhile to mention that the activation effects are much less significant for catalyst electrodes polarized at potentials less negative than −0.976 V vs RHE (Figure S12). The result suggests that the activation process may also be dependent on the oxidation state of the PorCu catalyst, with the reduced form being more likely to be activated.

The observed superior electrocatalytic performance in converting CO_2 to hydrocarbons directly reflects the properties of the PorCu molecular catalyst material. A set of control experiments were carried out to exclude the contribution from other species such as in situ formed Cu nanoparticles (Figure S13).[33] After 1 h of electrocatalysis at −0.976 V, the catalyst species on the PorCu catalyst electrode were washed with methanol. The methanol solution was examined by steady-state absorption and fluorescence spectroscopy (Figure S14). Based on the photophysical properties that the PorH gives intense fluorescent emission while Cu metalation completely quenches the fluorescence, the data show that ∼99% of the PorCu molecules survived the electrocatalysis process. The result was also confirmed by a MS test of the same methanol solution. Transmission electron microscopy (TEM) investigation revealed no formation of Cu nanoparticles (Figure S15). X-ray photoelectron spectroscopy (XPS) study verifies that Cu(II) remains as the dominant oxidation state after the electrocatalysis, further supporting the inexistence of Cu(0) nanoparticles (Figure S16). Furthermore, the methanol-washed electrode was reassembled into the reactor with the used electrolyte and polarized at −0.976 V vs RHE. The CO_2 reduction current density dramatically reduced to ∼1 mA cm^{-2} with a Faradaic efficiency of 6%, and CO was the dominant CO_2 reduction product (Figure S17), in striking contrast to the electrocatalytic performance of the original PorCu electrode. This unambiguously confirms that the PorCu molecules are the catalyst that converts CO_2 to hydrocarbons. It also verifies that the PorCu material catalyzes in a heterogeneous (as a solid catalyst layer on the electrode surface) rather than homogeneous (as molecules dissolved in the electrolyte) form in our reaction system.

The Cu center and built-in OH groups in the porphyrin structure are two indispensable factors for the distinct electrocatalytic performance of the PorCu catalyst. In a control experiment, the copper-free PorH material had hydrogen gas as the only product under the same CO_2 electroreduction measurement conditions (Figure S8), indicating that the Cu

center is the active site for electrochemical CO_2 reduction. We also found that a zinc(II)-porphyrin complex sharing the same porphyrin ligand as the PorCu dominantly produced hydrogen under identical electrochemical measurement conditions, which helps to exclude the possibility that reduced porphyrin may have catalyzed the CO_2-to-hydrocarbon reaction. We note that the distribution of CO_2 reduction products is clearly dependent on the applied electrode potential, and the hydrocarbon formation is strongly correlated with the reduction of the PorCu (Figures 3D and S18). Therefore, we conclude that the PorCu molecular structure with the Cu center in the +1 oxidation state is the active catalyst for electrochemically converting CO_2 to methane and ethylene.

In another control experiment, the OH-free PorCH3Cu material was examined under the same electrochemical measurement conditions (Figure S8). In addition to formic acid as the only liquid product with a Faradaic efficiency of 0.8%, CO was detected as the main gas-phase CO_2 reduction product with a Faradaic efficiency of <28%, and the maximum current density for CO_2 reduction was <0.7 mA cm^{-2} (Figure S19). The results clearly highlight the importance of the OH groups on the porphyrin structure for electrochemical reduction of CO_2 to hydrocarbons, perhaps by facilitating binding of certain reaction intermediates or by providing an intramolecular source of protons. However, the detailed mechanism is not clear at this moment and warrants further investigation.

In summary, we developed a new copper-porphyrin complex structure, which as a heterogeneous molecular catalyst delivers unprecedentedly high reaction rates of electrochemical CO_2 reduction to hydrocarbons (methane and ethylene) in aqueous media. The oxidation state of the Cu center and the built-in hydroxyl groups in porphyrin ligand have been identified to be critical factors contributing to the superior electrocatalytic performance of the material. Our study demonstrates the possibility of designing and tailoring molecular structures of metal-porphyrin complexes to promote heterogeneous electrocatalysis of CO_2 reduction.

■ ASSOCIATED CONTENT

Ⓢ Supporting Information

The Supporting Information is available free of charge on the ACS Publications website at DOI: 10.1021/jacs.6b04746.

     Detailed synthesis and data (PDF)

■ AUTHOR INFORMATION

Corresponding Authors
*hailiang.wang@yale.edu
*gary.brudvig@yale.edu

Author Contributions
‖These authors contributed equally.

Notes
The authors declare no competing financial interest.

■ ACKNOWLEDGMENTS

■ REFERENCES

(1) Qiao, J. L.; Liu, Y. Y.; Hong, F.; Zhang, J. *Chem. Soc. Rev.* **2014**, *43*, 631.

(2) Costentin, C.; Robert, M.; Saveant, J. M. *Acc. Chem. Res.* **2015**, *48*, 2996.

(3) Kortlever, R.; Shen, J.; Schouten, K. J.; Calle-Vallejo, F.; Koper, M. T. J. *J. Phys. Chem. Lett.* **2015**, *6*, 4073.

(4) Schouten, K. J. P.; Kwon, Y.; van der Ham, C. J. M.; Qin, Z.; Koper, M. T. M. *Chem. Sci.* **2011**, *2*, 1902.

(5) Lu, Q.; Rosen, J.; Jiao, F. *ChemCatChem* **2105**, *7*, 38.

(6) Gao, S.; Lin, Y.; Jiao, X. C.; Sun, Y. F.; Luo, Q. Q.; Zhang, W. H.; Li, D. Q.; Yang, J. L.; Xie, Y. *Nature* **2016**, *529*, 68.

(7) Lu, Q.; Rosen, J.; Zhou, Y.; Hutchings, G. S.; Kimmel, Y. C.; Chen, J. G. G.; Jiao, F. *Nat. Commun.* **2014**, *5*, 3242.

(8) Hori, Y. *Mod. Asp. Electrochem.* **2008**, *42*, 89.

(9) Chen, Y. H.; Kanan, M. W. *J. Am. Chem. Soc.* **2012**, *134*, 1986.

(10) Ren, D.; Deng, Y. L.; Handoko, A. D.; Chen, C. S.; Malkhandi, S.; Yeo, B. S. *ACS Catal.* **2015**, *5*, 2814.

(11) Asadi, M.; Kumar, B.; Behranginia, A.; Rosen, B. A.; Baskin, A.; Repnin, N.; Pisasale, D.; Phillips, P.; Zhu, W.; Haasch, R.; Klie, R. F.; Kral, P.; Abiade, J.; Salehi-Khojin, A. *Nat. Commun.* **2014**, *5*, 4470.

(12) Wu, J.; Yadav, R. M.; Liu, M.; Sharma, P. P.; Tiwary, C. S.; Ma, L.; Zou, X.; Zhou, X. D.; Yakobson, B. I.; Lou, J.; Ajayan, P. M. *ACS Nano* **2015**, *9*, 5364.

(13) Kumar, B.; Asadi, M.; Pisasale, D.; Sinha-Ray, S.; Rosen, B. A.; Haasch, R.; Abiade, J.; Yarin, A. L.; Salehi-Khojin, A. *Nat. Commun.* **2013**, *4*, 2819.

(14) Zhang, S.; Kang, P.; Ubnoske, S.; Brennaman, M. K.; Song, N.; House, R. L.; Glass, J. T.; Meyer, T. J. *J. Am. Chem. Soc.* **2014**, *136*, 7845.

(15) Saveant, J. M. *Chem. Rev.* **2008**, *108*, 2348.

(16) Collin, J. P.; Sauvage, J. P. *Coord. Chem. Rev.* **1989**, *93*, 245.

(17) Lin, S.; Diercks, C. S.; Zhang, Y. B.; Kornienko, N.; Nichols, E. M.; Zhao, Y. B.; Paris, A. R.; Kim, D.; Yang, P.; Yaghi, O. M.; Chang, C. J. *Science* **2015**, *349*, 1208.

(18) Kornienko, N.; Zhao, Y. B.; Kiley, C. S.; Zhu, C. H.; Kim, D.; Lin, S.; Chang, C. J.; Yaghi, O. M.; Yang, P. D. *J. Am. Chem. Soc.* **2015**, *137*, 14129.

(19) Costentin, C.; Drouet, S.; Robert, M.; Saveant, J. M. *Science* **2012**, *338*, 90.

(20) Furuya, N.; Matsui, K. *J. Electroanal. Chem. Interfacial Electrochem.* **1989**, *271*, 181.

(21) Magdesieva, T. V.; Yamamoto, T.; Tryk, D. A.; Fujishima, A. *J. Electrochem. Soc.* **2002**, *149*, D89.

(22) Kapusta, S.; Hackerman, N. *J. Electrochem. Soc.* **1984**, *131*, 1511.

(23) Sonoyama, N.; Kirii, M.; Sakata, T. *Electrochem. Commun.* **1999**, *1*, 213.

(24) Shen, J.; Kortlever, R.; Kas, R.; Birdja, Y. Y.; Diaz-Morales, O.; Kwon, Y.; Ledezma-Yanez, I.; Schouten, K. J. P.; Mul, G.; Koper, M. T. M. *Nat. Commun.* **2015**, *6*, 8177.

(25) Lindsey, J. S.; Schreiman, I. C.; Hsu, H. C.; Kearney, P. C.; Marguerettaz, A. M. *J. Org. Chem.* **1987**, *52*, 827.

(26) Lee, S.; Kim, D.; Lee, J. *Angew. Chem., Int. Ed.* **2015**, *54*, 14701.

(27) Kuhl, K. P.; Cave, E. R.; Abram, D. N.; Jaramillo, T. F. *Energy Environ. Sci.* **2012**, *5*, 7050.

(28) Manthiram, K.; Beberwyck, B. J.; Aivisatos, A. P. *J. Am. Chem. Soc.* **2014**, *136*, 13319.

(29) Li, C. W.; Kanan, M. W. *J. Am. Chem. Soc.* **2012**, *134*, 7231.

(30) Roberts, F. S.; Kuhl, K. P.; Nilsson, A. *Angew. Chem., Int. Ed.* **2015**, *54*, 5179.

(31) Reske, R.; Mistry, H.; Behafarid, F.; Cuenya, B. R.; Strasser, P. *J. Am. Chem. Soc.* **2014**, *136*, 6978.

(32) Weng, Z.; Su, Y.; Wang, D. W.; Li, F.; Du, J. H.; Cheng, H. M. *Adv. Energy Mater.* **2011**, *1*, 917.

(33) Wasmus, S.; Cattaneo, E.; Vielstich, W. *Electrochim. Acta* **1990**, *35*, 771.